6
Computational Modelling of the Magnetic Properties of Lanthanide Compounds

Liviu Ungur and Liviu F. Chibotaru

6.1
Introduction

Lanthanide ions are at the core of the most promising magnetic materials obtained to date. After the discovery of Ishikawa's terbium double decker $[Tb(Pc)_2]^-$ [1], the importance of lanthanide ions in the field of molecular magnetism grew rapidly [2, 3]. Significant effort has been made to rationalize the experimental results using traditional theoretical approaches, such as the phenomenological crystal field (CF) theory [4]. The growing amount of detailed experimental data on lanthanide compounds called for higher level theoretical tools for the description of their electronic and magnetic properties. In the recent years, explicitly correlated *ab initio* calculations, based on the complete active space self-consistent field (CASSCF) approach proved to be such a tool. Given its success in describing the magnetic properties of lanthanide compounds, we give here a thorough description of this *ab initio* methodology. The present chapter also revises several findings and insights in the field of lanthanide molecular magnetism obtained with the *ab initio* approach.

6.2
Ab Initio Description of Lanthanides and its Relation to Other Methods

A straightforward definition of the term *'ab initio'* is 'from the beginning', 'from the first principles'. *Ab initio* calculation of some property implies not using any experimental data or input, but relating the calculated property only to the fundamental constants entering the applied quantum-physical laws.

According to the basic principle of quantum mechanics, any measurable property can be computed *ab initio* if the total *wave function* ψ describing the quantum eigenstate of the system is known, since it contains the complete

Lanthanides and Actinides in Molecular Magnetism, First Edition.
Edited by Richard A. Layfield and Muralee Murugesu.

information about the system. It is obtained as a solution of the Schrödinger equation:

$$\hat{\mathbf{H}}\psi = E\psi \tag{6.1}$$

where $\hat{\mathbf{H}}$ is the energy operator of the system (the Hamiltonian), E is the energy eigenvalue and ψ is the eigenfunction. In the most general case, the Hamiltonian should include the kinetic energy of all particles, attraction between particles with opposite charges and repulsion between particles with identical charges, and account for relativistic effects (relativistic movement of the particles, the influence on their spin, orbital and magnetic moments, the interaction between the spin and orbital moments, etc.). Fully accounting for these interactions is an impossible task nowadays; therefore, several approximations are made in order to make the calculation feasible:

- Separation of the wave functions describing the motion of nuclei and the wave function describing the electrons (Born–Oppenheimer approximation). This approximation is based on the fact that the nuclear particles are much heavier than the electrons, and therefore much slower than the latter. In such a situation, the electronic wave function can be found at fixed positions of the nuclei.
- Representation of each molecular orbital as a linear combination of atomic orbitals (atomic basis sets). Atomic basis sets are usually represented as Slater type orbitals or as combinations of Gaussian functions. The latter is very popular, due to a very fast algorithm for the computation of bielectronic integrals.
- Treatment of the relativistic effects within the Douglass–Kroll–Hess (DKH) formalism [5–7], which is a reliable approximation for the much more complex Dirac equation for most atoms.
- Mean-field approximation of quasi-free electrons (the Hartree–Fock approximation). The total wave function is described, in this case, by a single Slater determinant.
- Accounting for electron correlation in a second step, via the mixing of a limited number of Slater determinants in the total wave function. Electron correlation is very important for correct treatment of interelectronic interactions and for a quantitative description of covalence effects and of the structure of multielectronic states. Accounting completely for the total electronic correlation is computationally extremely difficult, and is only possible for very small molecules, within a limited basis set. Formally, electron correlation can be divided into *static*, when all Slater determinants corresponding to all possible electron populations of frontier orbitals are considered, and *dynamic* correlation, which takes into account the effects of dynamical screening of interelectron interaction.

Further, we give a short review of the key points of the computational scheme suitable for the description of electronic structure in lanthanides.

6.2.1 *Ab Initio* Approach for the Electronic Structure of Lanthanides

The wave functions of the ground and excited states of lanthanides have a truly *multiconfigurational* character.[1)] Therefore, computational description of both the ground state and the low-lying excited states, which are important for magnetic behaviour, is only possible by a multiconfigurational *ab initio* method. In this respect, the CASSCF method proved to be a reliable tool for the description of electronic properties of lanthanide complexes.

6.2.1.1 Accounting for *Static* Electron Correlation within CASSCF

CASSCF is one of the most widely used *ab initio* multiconfigurational approaches [8–10]. It is based on an efficient partitioning of molecular orbitals into three main blocks: inactive (double-occupied), active and virtual (empty). The inactive orbitals are kept doubly occupied while the virtual orbitals are kept empty in all configurations employed to build the CASSCF wave function. The remaining electrons (active) span the explicitly correlated orbitals. The CASSCF wave function is a linear combination of all possible configurations (Slater determinants) which are built by following this partitioning scheme. Energy minimization is done self-consistently with respect to the coefficients of the Slater determinants (configuration interaction (CI) coefficients) and the molecular orbitals. A major limitation of the CASSCF calculation is the number of Slater determinants which are generated by a specific active space. In practice, the calculation becomes almost impossible if the wave function has more than 5–10 million configuration state functions (CSF, or Slater determinants), which is easily achieved for an active space consisting of 15–16 electrons spanning the same number of active orbitals. Various implementations aimed at lowering the number of the CSFs have been performed, the most promising one being the restricted active space self-consistent field (RASSCF) method [11, 12]. The success of the CASSCF method is due to its ability to describe near-degeneracies, which are often met for various problems, in particular, for the description of the near-degenerate ground states of transition metal (TM) and lanthanide compounds. Efficient implementations of the CASSCF methodology are present in MOLCAS [13], Gaussian [14], Orca [15], MOLPRO [16] and many other packages. In particular, it is the ability of the CASSCF method to describe near-degeneracies and excited states, which made it particularly suitable for the description of ligand-field states in lanthanide compounds.

6.2.1.2 Accounting for Dynamical Electron Correlation: An Important Step Towards Accurate Predictions

CASSCF wave function includes only the *static* correlation: only a small number of electrons spanning frontier orbitals are correlated between them, while

1) Except Gd^{3+}, which is a single-determinant due to its f^7 electronic configuration: $\Psi = |\uparrow\uparrow\uparrow\uparrow\uparrow\uparrow\uparrow|$

the correlation including inactive electrons also (which are usually much more numerous!), that is, the *dynamical* electron correlation, has to be accounted for in order to achieve accurate results. Currently there are two approaches for (partial) account of dynamical correlation to a multiconfigurational CASSCF wave function: (i) perturbative and (ii) CI methods.

Perturbative methods (CASPT2 [17], NEVPT2 [18]) add the dynamical correlation in an effective way, using multiconfigurational second-order perturbation theory on the CASSCF input states. These methods have proved to be suitable for studying problems in spectroscopy, photochemistry, and so on [19, 20].

CI methods [21] add a certain number of excited Slater determinants, usually selected by the excitation type (e.g. single, double, triple excitations), which were initially not present in the CASSCF wave function, and treat them in a non-perturbative way. Inclusion of additional configurations allows for more degrees of freedom in the total wave function, thus improving its overall description. These methods are extremely costly and therefore, are only applicable to small systems. Among this class of methods, DDCI (difference-dedicated configuration interaction) [22] and CISD (single- and double excitations) [21] are the most popular.

6.2.1.3 Accounting for Relativistic Effects within the Douglas–Kroll–Hess Theory

Accounting for relativistic effects exactly is only possible by solving the Dirac equation exactly. The original Dirac equation is of four components, which automatically means it is much more difficult to be solved than the Schrödinger equation (6.1). Transformations employed by Douglas and Kroll [23] together with the so-called 'decoupling scheme' employed by Hess [24, 25] allowed for a much simpler and practical way to account for relativistic effects without the need to solve the complete system of Dirac equations. In this treatment, the relativistic effects are divided into two parts: the scalar contribution and the spin–orbit coupling. Scalar relativistic corrections are accounted for in the basis set generation, when effective-core potentials (ECPs) or atomic natural orbitals with relativistic correction (e.g. ANO-RCC [26, 27] or ANO-DK3 [28]) are employed for the description of individual atoms. Accuracy in the treatment of relativistic effects can be achieved by gradually increasing the order of the DKH expansion [7]. However, for most chemical elements, treatment of relativistic effects in the second-order DKH expansion is sufficient. Practical implementations of the second-order DKH are present in almost all quantum chemical packages. For the computation of lanthanides, an important aspect is the accuracy of the spin–orbit coupling treatment. For complexes with the ground orbital state well separated from excited states, when the energy separation is several times larger than the spin–orbit coupling, magnetic properties are reasonably well described by treating spin–orbit coupling perturbatively. In the opposite case, when the spin–orbit coupling is larger than the energies of few excited orbital states, for example, in the near-degenerate cases (almost all lanthanide compounds),

perturbative treatment of the spin–orbit coupling fails to describe correctly the electronic and magnetic properties. In the MOLCAS program package [13], spin–orbit coupling is treated non-perturbatively within the mean-field theory in the restricted active space state interaction (RASSI) method [29]. In this method, the spin–orbit state-interaction matrix is built on the basis of the input states optimized at the CASSCF level. Diagonal energies of the state interaction matrix can be those of the initial CASSCF calculation or taken from a more advanced CASPT2 calculation. Diagonalization of the spin–orbit matrix leads to spin–orbit multiplets.

It is important to mention that the RASSI method treats all wave functions as 'frozen', that is, the CASSCF wave functions do not change during the calculation. Allowing the relaxation of the CASSCF wave functions during the RASSI step, would, probably, improve the results. There are several attempts to consider spin–orbit coupling in a variational way [30–32]. The main drawback of the methods involving variational treatment of spin–orbit coupling is that the dynamical correlation becomes effectively impossible to be treated, either perturbatively or by CI. The reason for this is the large number of spin orbitals, which is doubled compared to the number of orbitals in the non-relativistic methods.

6.2.1.4 Spin–Orbit Multiplets of Free Lanthanide Ions: Relativistic CASSCF/RASSI Method in Work

Owing to the fact that a correct description of the spin–orbit coupling for lanthanides requires a large number of spin terms to be included in the calculation, it is computationally very difficult to include dynamical correlation for them in the case of real lanthanide compounds, irrespective of the approach. On the other hand, since most of the excited states of lanthanide compounds, important for the magnetism, are of ligand-field type (various arrangements of n electrons within the 4f shell) the dynamical correlation is expected to be of similar importance for the entire ground atomic term, leading to minor relative energy changes for the low-lying J-multiplets compared to a CASSCF/RASSI calculation. In fact, as we show in Table 6.1, minimal relativistic CASSCF/RASSI calculations give already quite accurate energies of low-lying multiplets which are responsible for magnetism, in all lanthanides. This agreement, however, is not as good for excited terms as it is for the ground one presented in the Table 6.1. This is seen, for example, in the comparison between experimental and calculated J-multiplets originating from the excited ^{6}P atomic term of the Gd^{3+} ion. For an accurate description of higher excited J-multiplets, originating from excited atomic terms, dynamical correlation is very important and should not be neglected.

In lanthanide complexes, the ligand field created by the surrounding ligands will split the atomic J-multiplets into several components. The latter are doubly degenerate (Kramers doublets (KDs)) for systems with odd number of electrons and non-degenerate (in the absence of symmetry) for systems with even number of electrons.

Table 6.1 Energies of the low-lying *J*-multiplets predicted within the CASSCF/RASSI approach for the free Ln^{3+} ions. ANO-RCC of single-zeta quality were employed. The active space of the CASSCF method included only *n* electrons spanning the 4f shell.

	Term	*J*-multiplet	Experiment [33]	Calculation		*J*-multiplet	Experiment [33]	Calculation
Ce^{3+}, f^1	^2F	5/2	0	0	Yb^{3+}, f^{13}	7/2	0	0
		7/2	2 253	2 415		5/2	10 214	9 771
Pr^{3+}, f^2	^3H	4	0	0	Tm^{3+}, f^{12}	6	0	0
		5	2 152	2 120		5	8 090	7 952
		6	4 389	4 359		4	12 500	12 724
Nd^{3+}, f^3	^4I	9/2	0	0	Er^{3+}, f^{11}	15/2	0	0
		11/2	1 880	1 841		13/2	6 480	6 290
		13/2	3 860	3 835		11/2	10 110	10 138
		15/2	5 910	5 939		9/2	12 350	12 807
Pm^{3+}, f^4	^5I	4	0	0	Ho^{3+}, f^4	8	0	0
		5	1 490	1 442		7	5 050	4 887
		6	3 110	3 045		6	8 550	8 412
		7	4 820	4 763		5	11 110	11 048
		8	6 580	6 559		4	13 180	13 109
Sm^{3+}, f^5	^6H	5/2	0	0	Dy^{3+}, f^5	15/2	0	0
		7/2	1 080	1 011		13/2	3 460	3 349
		9/2	2 290	2 213		11/2	5 780	5 734
		11/2	3 610	3 557		9/2	—	7 579
		13/2	4 990	5 004		7/2	9 060	9 007
		15/2	6 470	6 518		5/2	10 100	10 070
Eu^{3+}, f^6	^7F	0	0	0	Tb^{3+}, f^6	6	0	0
		1	370	353		5	2 052	1 982
		2	1 040	989		4	3 314	3 263
		3	1 890	1 828		3	4 292	4 242
		4	2 860	2 806		2	4 977	4 940
		5	3 910	3 874		1	5 431	5 400
		6	4 940	4 998		0	5 653	5 626
Gd^{3+}, f^7	^8S	7/2	0	0				
	^6P	7/2	32 120	39 406				
		5/2	32 720	39 927				
		3/2	33 290	40 474				

6.2.2
Ab Initio Versus Two-Component DFT

Two-component DFT methods aim at solving the reduced form of the four-component Dirac equation using DFT formalism. The full relativistic treatment allows describing, for instance, a noncollinear magnetic density in the ground state of complexes [34]. Although relativistic effects are accurately described by these methods, an adequate solution is only obtained for wave functions which could be represented by a single Slater determinant. In this respect, two-component DFT methods are not applicable for the description of electronic properties of lanthanides, since the wave function for most of them has an intrinsic multideterminantal character. In the case of lanthanides (f^n system) we have the following situations:

- For $n < 7$, the total spin of the system S couples antiferromagnetically with the orbital momentum L into the total momentum in the ground state: $J = |L - S|$ [35]. The individual $|J, M_J\rangle$ multiplets cannot be, in principle, described by a single Slater determinant. This is a consequence of the general rules of coupling of two angular momenta: eigenfunctions of all projections of the total angular momentum $|J, M_J\rangle$, which is lower than the maximal possible $(L + S)$, are represented as linear combinations of several determinants [36].
- For $n = 7$, the case of Gd^{3+}, the ground term is orbitally non-degenerate ($L = 0$). Then, $J = S$ and the ground state wave function is adequately described by a single Slater determinant, that is, DFT methods may work.
- For $n > 7$, the spin–orbit interaction stabilizes the maximal total momentum in the ground state, $J = L + S$ [35]. Depending on the character of the splitting of the ground J-multiplet, the following situations may occur:
  - $M_J < M_{J\max}$ – the wave function is multideterminantal.
  - $M_J = M_{J\max}$ – this is the only case, which can, in principle, lead to a single-determinant wave function. This situation may be encountered in some limited highly axial systems, such as Dy-O^+ [37]. However, usual compounds do not have any site symmetry, which means that several projections of the J-manifold will be mixed by the low-symmetry components of the CF, leading to a multideterminantal character of the wave function.

In conclusion, the DFT approach, even in a two-component scheme, is generally not applicable to treat lanthanides.

6.2.3
Ab Initio Versus Phenomenological Crystal Field Theory for Lanthanides

CF (ligand field) theory was one of the first theoretical tools employed for rationalization of experimental data for lanthanide compounds. There are two different CF approaches employed for the description of lanthanide complexes: (i)

the phenomenological treatment of the lowest J-multiplet involving effective CF parameters specific for this group of states [38, 39] and (ii) the microscopic CF model, which considers all single- and bielectronic interactions in the f^n shell [4, 40, 41]. However, both these approaches can give only a limited insight into the nature of ligand field states due to the following reasons:

- The relative contributions of covalent, electrostatic and other interactions to the CF are not known a priori. The existent models include exclusively either covalent (angular overlap model [42–44] or electrostatic [40, 41, 45] interactions, which seems unjustified.)
- The 'effective' CF models, intended to include covalence effects via effective charges and shielding parameters [46] (superposition model [47], effective charge model [48], simple overlap model [49, 50]), keep the radial ($M-L$ distance) dependence of the CF parameters as in the simple (point charge) electrostatic model. Dedicated studies have shown, however, that the radial dependence of these parameters deviates strongly from the latter for the whole series of lanthanide ions [51, 52].
- The existent CF models neglect or describe very approximately the effect of multiatomic structure, conjugation and multidentate character of the ligand on the CF parameters. The effect of second and more distant coordination spheres is described as electrostatic, in some models, while it was proved by *ab initio* calculations that it is mainly covalent by its nature [53, 54].
- The bottleneck of phenomenological models is the large number of independent parameters (27 in low-symmetric complexes) required for the description of the CF, which cannot be reliably extracted from experiment in a unique manner. As a rule, these models are confronted with the description of a limited amount of experimental data, while it is not possible in principle to provide the entire set of CF parameters. The latter strongly depend on fitted experiments and, therefore, are not reliable (an example is described below).

6.3 *Ab Initio* Calculation of Anisotropic Magnetic Properties of Mononuclear Complexes

The increased power of *ab initio* methods underlay an important progress manifested in two aspects. First, they allow nowadays treating large complexes (with more than a hundred of atoms) fully *ab initio*. Second, these methods provide accurate solutions for multielectronic eigenstates, which often allows making predictions of different properties of complexes with an experimental accuracy. Representative quantum chemistry software is the MOLCAS package [13]. As was mentioned before in Section 6.2.1, the DKH treatment of relativistic effects in combination with explicitly correlated multiconfigurational description of the multielectronic wave functions provides very good solutions for molecular multiplets of the complexes. The latter can be used in principle for the calculation

of magnetic properties of different complexes. Indeed, since these properties are simply a response to a Zeeman interaction induced by an external magnetic field **B**, in order to evaluate them, we only need to know the matrix elements of the operator of total magnetic moment of the complex $\hat{\boldsymbol{\mu}}$ calculated on the basis of multiplet eigenstates.

$$\hat{\mathbf{H}}_{\mathrm{Zee}} = -\hat{\boldsymbol{\mu}}\mathbf{B}, \;\; \hat{\boldsymbol{\mu}} = -\mu_{\mathrm{B}} \sum_{i=1}^{N_{\mathrm{el}}} g_{\mathrm{e}} \hat{\mathbf{s}}_i + \hat{\mathbf{l}}_i \tag{6.2}$$

6.3.1 Implementation of *Ab Initio* Methodology: SINGLE_ANISO Program

The SINGLE_ANISO program is a routine which allows for non-perturbative calculation of effective spin (pseudospin) Hamiltonians and static magnetic properties of mononuclear complexes and fragments completely *ab initio*, including the spin–orbit interaction. As a starting point, it uses the results of a CASSCF/(CASPT2)/RASSI calculation for the ground and several excited spin–orbit multiplets. A description of the computational methodology of pseudospin Hamiltonians is given in [55, 56] while the derivation of (macroscopic) magnetic properties is given in [57].

The SINGLE_ANISO program is able to calculate the following:

- Parameters of pseudospin magnetic Hamiltonians:
  1. First rank (linear after pseudospin) Zeeman splitting tensor $g_{\alpha\beta}$ (i.e., the conventional g tensor), its main values, including the sign of the product $g_X g_Y g_Z$, and the main magnetic axes (X_m, Y_m, Z_m) in the initial coordinate frame.
  2. Second rank (bilinear after pseudospin) zero-field splitting tensor $D_{\alpha\beta}$ (i.e. the conventional D tensor), its main values and the main anisotropy axes (X_a, Y_a, Z_a).
  3. Higher rank ZFS tensors (D^4, D^6, ... , etc.) and Zeeman splitting tensors (G^3, G^5, ... , etc.) for complexes with moderate and strong spin–orbit coupling.
  4. Angular moments along the main magnetic axes.

  Magnetic Hamiltonians are defined for a desired group of N electronic states obtained in the *ab initio* calculation, to which a pseudospin $\tilde{S}$ (it reduces to a true spin S in the absence of spin–orbit coupling) is subscribed according to the relation $N = 2\tilde{S} + 1$. For instance, the two wave functions of a KD correspond to $\tilde{S} = 1/2$. The implementation is done for *any dimension* of the pseudospin.
- A complete decomposition of the *ab initio* computed CF matrix in irreducible tensor operators (ITOs) and in extended Stevens operators. The parameters of the multiplet-specific CF acting on the ground atomic multiplet of lanthanides, and the decomposition of the CASSCF/RASSI wave functions into functions with definite projections of the total angular momentum on the quantization axis are provided.

- Static magnetic properties:
  1. Van Vleck susceptibility tensor $\chi_{\alpha\beta}(T)$
  2. Powder magnetic susceptibility function $\chi(T)$
  3. Magnetization vector $\vec{\mathbf{M}}(\vec{\mathbf{B}})$ for specified directions of external magnetic field $\vec{\mathbf{B}}$
  4. Powder magnetization $M_{\mathrm{mol}}(B)$

The calculation of magnetic properties takes into account the contribution of excited states (the ligand-field and charge transfer states of the complex or mononuclear fragment included in the RASSI calculation) via their thermal population and Zeeman admixture. The intermolecular exchange interaction between magnetic molecules in a crystal can be taken into account during the simulation of magnetic properties by a phenomenological parameter zJ' specified in the input.

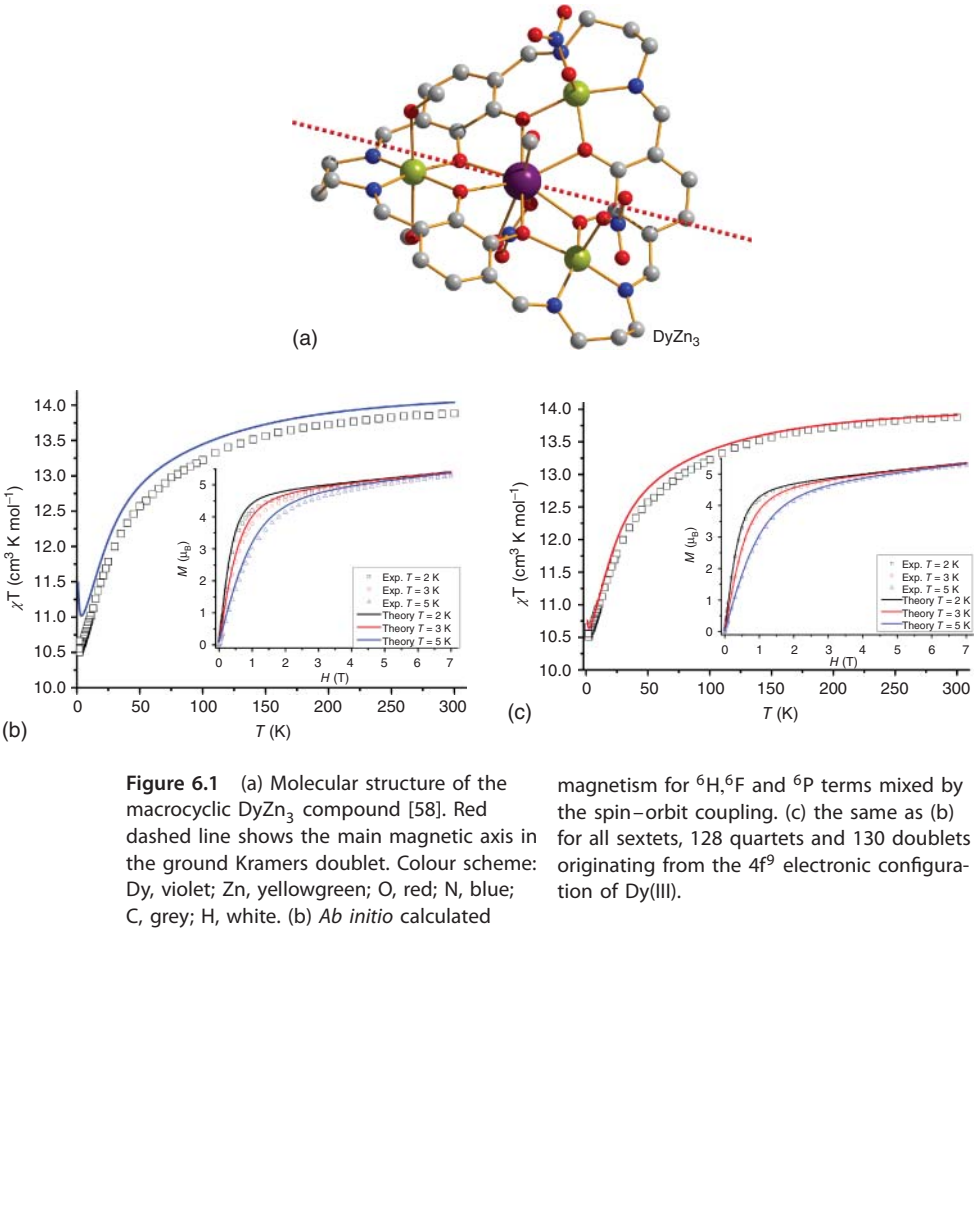

Figure 6.1 (a) Molecular structure of the macrocyclic $DyZn_3$ compound [58]. Red dashed line shows the main magnetic axis in the ground Kramers doublet. Colour scheme: Dy, violet; Zn, yellowgreen; O, red; N, blue; C, grey; H, white. (b) *Ab initio* calculated magnetism for ^{6}H,^{6}F and ^{6}P terms mixed by the spin–orbit coupling. (c) the same as (b) for all sextets, 128 quartets and 130 doublets originating from the $4f^9$ electronic configuration of Dy(III).

6.3.2
Temperature-Dependent Magnetic Susceptibility and Field-Dependent Magnetization

An example of the application of relativistic CASSCF/RASSI/SINGLE_ANISO calculations for the description of magnetism of lanthanide complexes is the recently studied $DyZn_3$ compound (Figure 6.1) [58]. All three Zn^{2+} ions have a $3d^{10}4s^0$ electronic configuration in the ground state, which means that they are non-magnetic ($S = 0$). This makes the $DyZn_3$ complex magnetically equivalent to a mononuclear Dy complex, since the magnetism of this compound is solely due to the presence of the Dy^{3+} ion, which has a $4f^95d^06s^0$ open-shell electronic configuration. Table 6.2 shows the results of the *ab initio* CASSCF/RASSI calculations. These calculations have been performed using ANO-RCC basis sets of the following contractions: [8s7p5d4f2g1h] for Dy, [5s4p2d1f] for Zn, [4s3p1d] for O and N from the first coordination sphere, [3s2p] for C, and all remaining N and O, and [2s] for H; the active space of the CASSCF method included nine electrons spanning seven 4f orbitals, CAS (9 in 7). The number of states included in the spin–orbit mixing was gradually increased from the minimal one (^{6}H, ^{6}F and ^{6}P, 21 spin states) towards the maximal possible one (279 spin states, limited by the hardware). We see that a minimal description of the spin–orbit coupling gives already a reasonable description of the magnetism, while the mixing of a large number of spin terms leads to a much better description of magnetism.

Table 6.2 Energies of the lowest spin-free states originating from the ^{6}H multiplet and the energies of the low-lying Kramers doublets of the $DyZn_3$ complex.

Atomic multiplet	Spin free states	*J* multiplet	Kramers Doublets
	0.0		0.0
	29.1		41.7
	88.3		75.4
	95.6		217.7
	173.8	$\frac{15}{2}$	273.6
^{6}H	192.9		298.9
	365.4		343.1
	387.1		391.9
	497.3		
	538.6		
	581.7		
Main values of the g tensor in the ground Kramers doublet			
g_X			0.105
g_Y			0.255
g_Z			18.148
Sign of the $g_Xg_Yg_Z$			+

6.3.3 Magnetic Anisotropy in Low-Lying Doublets

The ground atomic J-multiplet of a lanthanide ion f^n splits in low-symmetry complexes into $2J + 1$ non-degenerate for even n (usually grouped in doublets), and in $(2J + 1)/2$ degenerate KDs for odd n. The *ab initio* calculations described above should be able to describe adequately the magnetic anisotropy of these doublet states. This was indeed found to be the case for individual Dy centres in Dy_3 triangles [59], for which *ab initio* calculations predicted the directions of local anisotropy axes [60] very close to the experimental results [61]. An example of a mononuclear Ln complex for which an ample comparison of experimentally measured single-ion magnetic anisotropy with *ab initio* predictions has been performed is the recently investigated Cp*ErCOT single-molecule magnet (SMM) [62]. Figure 6.2 shows the polar plot of angular dependence of single-crystal magnetization in the $a - b$ plane for each of the two molecules in the unit cell of the crystal. The relative shift of the theoretical plots from the experimental ones is due to the deviation of the calculated main anisotropy axes on the two molecules from the experimental ones by a few degrees [62]. Comparable accuracy of the *ab initio* calculated directions of local anisotropy axes has been demonstrated for other mononuclear lanthanide complexes as well by direct comparisons with the results of single-crystal investigations [54, 63, 64]. An indirect indication of the high accuracy of the predictions of local anisotropy axes in *ab initio* calculations of mononuclear Ln fragments (see the next section) can be inferred from good reproduction of magnetic properties of polynuclear lanthanide complexes, which crucially depend on relative orientations of these axes [65–75].

An important feature of the lanthanides is the *high axiality* of ground doublet state often achieved even in low-symmetry Ln complexes and fragments. This means a much larger g factor along the easy axis compared to hard axes (transversal g factors) in the case of Ln ions with odd number of electrons, and small splitting of the ground doublet in the case of Ln ions with even number of electrons. The high axiality of the ground doublet state explains the suppression of quantum tunnelling of magnetization (QTM) and the SMM behaviour of most of the lanthanide complexes, even when they completely lack any symmetry [37]. As an example, Table 6.3 shows that the transversal g factors (g_X, g_Y), for a low symmetry Dy(III) fragment of a Dy_3 triangle [37] are very small for the ground state KD1, that is, it is strongly axial. The table shows that for higher doublets the axiality strongly diminishes, becoming the lowest in the middle of the spectrum, while starting to increase again for the highest states. Concomitantly, the main anisotropy axes of the doublet state gradually rotate with respect to each other [37]. A similar behaviour is observed for Ln ions with even number of electrons in low-symmetry environment. Table 6.4 shows the results of *ab initio* calculations for a Tb(III) centre in the Tb_3 complex [76]. We see again that the lowest and the highest Ising doublets exhibit the smallest splitting (i.e. show the highest axiality),

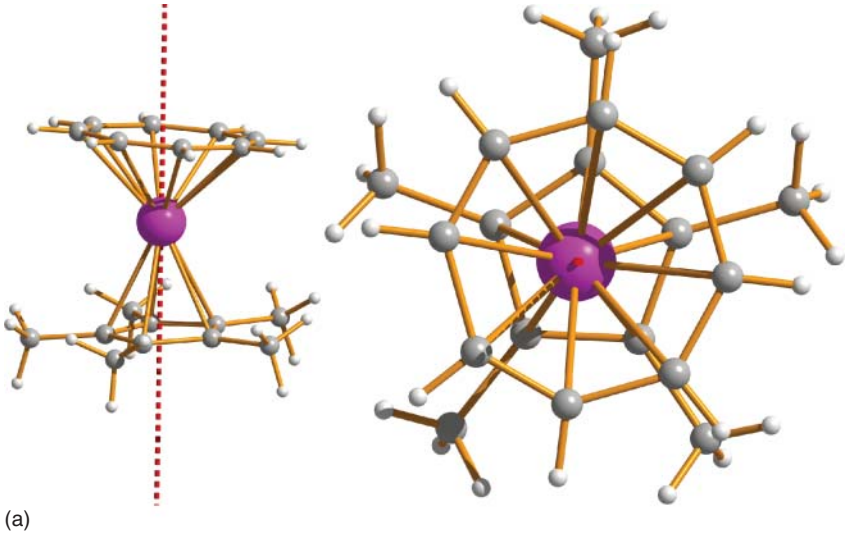

(a)

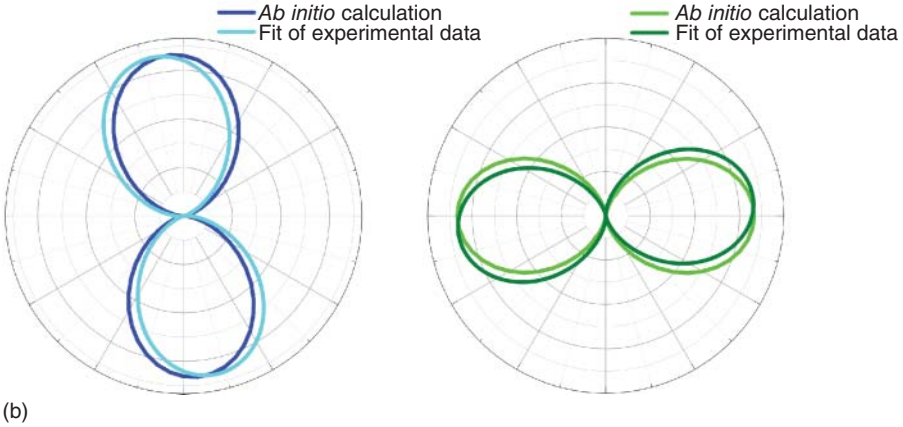

(b)

Figure 6.2 (a) Orientation of the main magnetic axis in the ground Kramers doublet of [Cp*ErCOT], [62]. Colour scheme: Er, purple; C, yellow; H, white. (b) Polar plot of the angular dependence of the single-crystal magnetic susceptibility recorded in the *a*–*b* plane, comparison between the results of the *ab initio* calculation for two molecules in the unit cell (left and right plot, respectively) and the contributions extracted from the fit of the experimental data (colour code in insets).

while the main magnetic axes rotate gradually when passing from one doublet to the other [37]. We stress that the almost perfect axiality of the ground doublet state of low-symmetry lanthanide centres is an important feature enabling them to function as SMM. This is especially important in polynuclear complexes where Ln centres do not have, as a rule, any site symmetry.

Table 6.3 Energies (per centimetre) and main values of the g tensors of the lowest Kramers doublets at the Dy_3 site of the dysprosium triangle (from [37]).

Kramers doublet	Energy	g_X	g_Y	g_Z
1	0.000	0.008	0.034	19.667
2	103.476	0.398	0.645	17.750
3	141.038	3.495	3.670	11.366
4	171.100	2.214	4.969	11.748
5	208.691	0.069	3.223	14.098
6	228.586	1.215	3.047	16.450
7	287.051	0.104	0.281	18.743
8	395.074	0.002	0.008	19.556

Source: From Ref. [37].

Table 6.4 Energies (per centimetre) and the g_Z values[a)] of the lowest Ising doublets at the Tb_3 site of the Tb_3 complex

Ising doublet	Energy	Δ_{tun}	g_Z
1	0.000	0.090	17.837
	0.090		
2	106.225	1.271	14.711
	107.496		
3	171.446	6.940	11.853
	178.386		
4	214.780	—	—
5	235.191	7.797	9.904
	242.988		
6	275.819	1.693	14.113
	277.512		
7	485.772	0.046	17.685
	485.818		

a) $g_X = g_Y = 0$ according to the Griffith's theorem [77].
Source: From Ref. [37].

6.3.4
Ab Initio Crystal Field

As was mentioned in Section 6.2.3, phenomenological CF models have been extensively used in the past to rationalize the electronic structure of lanthanide complexes [4, 40–50], and they are still in use nowadays [38, 39, 78, 79]. The *ab initio* approach described above is, in principle, able to provide accurate energies and wave functions of multiplets in lanthanide complexes. Nevertheless, even if *ab initio* calculations appear to be successful, CF description is still of great

interest because it includes in a concentrated way all basic interactions responsible for magnetic and optical (luminescence) properties of lanthanides. In this sense, the parameters of CF Hamiltonians play the role of physical characteristics of the complexes, much similar to the parameters of the effective zero-field splitting and how Zeeman Hamiltonians do for their magnetic properties. For the latter, the most relevant is the CF splitting of the ground atomic J-multiplet, that is, the multiplet-specific CF Hamiltonian:

$$\hat{\mathbf{H}}_{\mathrm{CF}}^{J} = \sum_{n,m} (B_n^m O_n^m \left(\frac{\hat{\mathbf{J}}}{J}\right) + C_n^m \Omega_n^m \left(\frac{\hat{\mathbf{J}}}{J}\right) \tag{6.3}$$

where O_n^m and Ω_n^m are Stevens operators [35] defined in the space of angular momentum operator $\hat{\mathbf{J}}$ of the ground atomic multiplet. We have developed recently an approach based on ITO projection, which allows a unique determination of all 27 parameters B_n^m and C_n^m entering equation 6.3 from the *ab initio* calculations described above [80]. We stress that this is the only way to derive the set of *true* CF parameters, which would not be the case if a fitting procedure would have been applied. Another advantage of this procedure is that it permits to project out the CF contribution (6.3) from the total energy matrix and to assess the importance of higher rank ($n > 6$) non-CF contributions. This methodology is currently implemented in the SINGLE_ANISO module [81] of the MOLCAS program package [13] and can be used routinely.

As an example, we consider the Ishikawa's terbium double decker exhibiting an SMM behaviour, $[Tb(Pc)_2]^-$, where Pc is phtalocyanine [38]. Figure 6.3 shows the calculated spectrum of levels originating from the ground $J = 6$ multiplet of Tb(III) for the experimental geometry. The corresponding CF parameters calculated with SINGLE_ANISO routine as described above are shown in Table 6.5 [80]. This CF analysis also shows that the ground doublet state is very close to $M_J = \pm 6$ origin, while the first excited doublet is predominantly of $M_J = \pm 5$ type. For comparison, in Figure 6.3 is shown the spectrum obtained by phenomenological CF model involving only three axial parameters (Table 6.5) extracted from the fitting of magnetic susceptibility and of the chemical shift [1]. Although the nature of the ground and first excited doublet obtained is the same as in *ab initio* calculations, the energy separation is quite different, being closer to the experimental value (260 cm^{-1}) [1] in the latter case. The discrepancy between the two spectra becomes larger for the excited states. Another important observation is the very strong dependence of the CF spectrum on the deviation from the ideal symmetry. Although $[Tb(Pc)_2]^-$ is considered as a prototype of a high-symmetry Ln complex showing deviations from an ideal D_{4d} geometry of hundredths of angstroms in the Ln–N bond lengths, its symmetrization results in strong reconstruction of the *ab initio* spectrum (Figure 6.3). This is also seen in the strong difference between the CF parameters corresponding to the real and symmetrized geometries (Table 6.5). Obviously, such sensitivity of the CF at Ln ions on the geometry of their environment can hardly be simulated

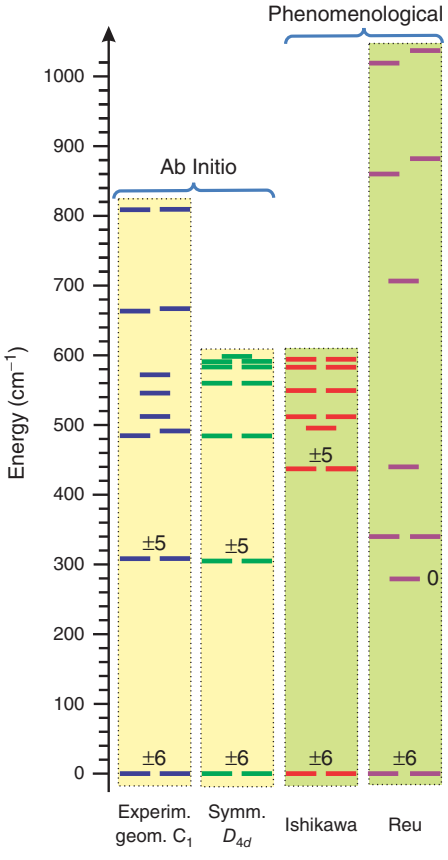

Figure 6.3 Comparison between ligand field states of the $[Tb(Pc)_2]^-$ obtained *ab initio* for the real geometry, for the symmetrized geometry up to the D_{4d} point group symmetry, and extracted from the fitting of the experimental data within CF approaches of Ishikawa [1] and Reu [78], assuming that the $[Tb(Pc)_2]^-$ compound has exact D_{4d} and C_4 symmetry, respectively.

realistically by phenomenological models. As an example, we show in Figure 6.3 the calculated CF spectrum for symmetrized $[Tb(Pc)_2]^-$ within the exchange charge model of the CF [78]. Despite the fact that the parameters in this model have been fitted to the same experimental data as in the previous CF model [1], the CF spectrum of the two models differ drastically. In particular, the first excited state predicted by the exchange charge model corresponds to the $M_J = 0$ [78] and not to the $M_J = \pm 5$ predicted by the previous CF model (and the *ab initio* calculations). This comparison shows that phenomenological CF models can encounter serious problems in the prediction of realistic spectrum so that the

Table 6.5 Crystal-field parameters for Ishikawa's $[Tb(Pc)_2]^-$ complex obtained *ab initio* for the experimental geometry [80], for the symmetrized geometry [80] and those obtained from the fitting of the experimental data [1, 78].

Rank	Projection	Real geometry		D_{4d}- geometry		Fitting by Ishikawa [1]		Fitting by Reu[78]	
		B_n^m	C_n^m	B_n^m	C_n^m	B_n^m	C_n^m	B_n^m	C_n^m
2	0	608.8	–	530.4	–	414	–	173	–
	1	−19.1	4.6	0	0	x	x	*x*	x
	2	19.2	317.9	0	0	x	x	*x*	x
4	0	−98.5	–	−112.1	–	−228	–	−631.4	–
	1	−11	0.5	0	0	x	x	*x*	x
	2	3.5	59.8	0	0	x	x	*x*	x
	3	0.6	−2.2	0	0	x	x	*x*	x
	4	−15	5	0	0	x	x	397.4	953
6	0	−13.9	–	−7.5	–	33	–	79.7	–
	1	−0.2	−0.9	0	0	x	x	*x*	x
	2	−0.7	24.1	0	0	x	x	*x*	x
	3	1.3	−1.2	0	0	x	x	*x*	x
	4	−5.3	3	0	0	x	x	256.4	667
	5	3.4	−4.1	0	0	x	x	*x*	x
	6	12.1	17.9	0	0	x	x	*x*	x

x – parameters that were ignored in the fitting of experimental data [1, 78];

ab initio approach becomes indispensable, especially, when all 27 CF parameters are non-negligible.

6.4 *Ab Initio* Calculation of Anisotropic Magnetic Properties of Polynuclear Complexes

The *ab initio* calculations of the exchange spectrum and the derivation of exchange parameters for polynuclear lanthanide complexes is a much more difficult task than the calculation of CF splitting and single-ion magnetism. This is the reason why such calculations have not yet been done. DFT calculations of exchange coupling parameters have been done only for Gd-TM and Gd-radical (R) complexes [82], but cannot be applied to other lanthanide ions due to reasons mentioned in Section 6.2.2. Fortunately, the exchange interactions between two strongly axial lanthanide ions (Ln1 – Ln2) or between a strongly axial lanthanide ion and an isotropic spin, such as Ln-TM, or Ln-R exchange coupled pairs, reduces the exchange interaction of the Ising type for the ground doublet states. The latter can be efficiently described within a semiempirical two-step approach reviewed in subsequent sections.

6.4.1 Two-Step Approach for the Calculation of Electronic Structure of Polynuclear Lanthanide Complexes

Localization of the magnetic orbitals observed in TM complexes and networks [83] is even more pronounced in lanthanide-containing mono- and polynuclear compounds. This fact allows treating the electronic and magnetic structure of polynuclear compounds in a two-step procedure. In the first step, reasonable fragmentation of the cluster into mononuclear fragments is performed and reliable *ab initio* calculations for each fragment are done. In the second step, the magnetic interaction between the fragments is introduced in an effective way. The exchange interaction between magnetic centres is considered within the Lines model [84], while accounting for the dipole–dipole magnetic coupling is treated exactly. The Lines model [84] is an approximation that allows describing the anisotropic exchange interaction between magnetic sites via a single parameter. To this end, an isotropic Heisenberg model involving the true spins of the two centres is introduced with an effective parameter (the Lines exchange parameter). In the second step, the matrix of this model is constructed on the basis of products of localized lowest states of the two centres obtained in fragment *ab initio* calculations of corresponding centres with spin–orbit coupling included. The exchange matrix obtained describes exactly the anisotropic exchange interaction in two limiting cases:

1) Of two strongly axial doublets on the two sites (the case of extreme magnetic anisotropy)
2) Of isotropic spins on the two sites (lack of magnetic anisotropy).

The Lines approximation is expected to be quite accurate for the description of the exchange interaction between a strongly axial doublet and an arbitrary isotropic spin. For all other cases, the Lines model [84] is a reasonable approximation. Efficient implementation of the Lines model was done in the program POLY_ANISO.

6.4.2 Key Rules for Cluster Fragmentation

One important point in this two-step approach is the cluster fragmentation into mononuclear fragments containing unpaired electrons (spins) only on one magnetic centre. By fragmentation, we try to achieve the preservation of the electronic and magnetic structure of each of the magnetic centres as close as possible to their form in the initial polynuclear cluster (if one makes abstraction of relatively weak exchange and dipolar interaction between the sites).

From previous experience, one can formulate some rules for building reliable fragments:

- If the computer power is sufficient, it is not recommended to remove any atom from the initial polynuclear molecule. To calculate the magnetic states on one centre, neighbouring metal ions have to be described by their closest diamagnetic equivalents. For example, Fe^{2+}, Co^{2+}, Ni^{2+} and Cu^{2+} could be reasonably well described by diamagnetic Zn^{2+}, while Ti^{2+}, V^{2+}, Cr^{2+} and Mn^{2+} are probably better described by diamagnetic Ca^{2+}. In this respect, the charge of the neighbouring ions should also be taken into account correctly: Ti^{3+}, V^{3+}, Cr^{3+} and Mn^{3+} can be simulated by diamagnetic Sc^{3+}. Metals which are known to have a very stable closed-shell (i.e. diamagnetic) configuration in the ground state (e.g. octahedral Co^{3+}) are recommended to be kept as they are in the *ab initio* calculation.
- If the cluster is too large to be treated as described above, then some distant groups of atoms have to be removed or replaced. It is always recommended to start the removal of atomic groups from distant regions of the considered magnetic centre. At this step chemical intuition is of great help. For example, $-CH_3$ group is chemically quite similar to the H atom; therefore, such a substitution at a significant distance from the magnetic centre is not supposed to change the electronic and magnetic structure on the metal site much. *t*-Butyl groups could be efficiently modelled by a $-CH_3$ group. However, it is not accurate, in our opinion, to replace conjugated rings (e.g. phenyl) by H atoms, as they are quite large, and may induce $\pi-\pi$ stacking effects, which influence intra- and intermolecular magnetic interactions. Such a replacement is acceptable only for a crude computational model. In general, it is better to avoid breaking of any conjugated part of the molecule, or to cut the double or triple bond.
- The position of the hydrogen atoms which are bonded directly to the first-coordinated ligand atoms (usually O, N) is very important, as they effectively orient the orbitals of the first-coordinated ligand atoms, influencing directly the ligand field acting on the magnetic centre. In general, the effect of the second coordination sphere is of great importance for the correct description of the ligand field, as has been previously shown [53, 85].

6.4.3 Implementation of *Ab Initio* Methodology: POLY_ANISO Program

The POLY_ANISO program is a computational tool which allows treatment of exchange interaction within the Lines model, dipole–dipole magnetic coupling, calculation of effective spin (pseudospin) Hamiltonians and static magnetic properties of polynuclear complexes using the *ab initio* calculated wave functions and spectrum of individual magnetic centres (fragments). The computational methodology for pseudospin Hamiltonians is similar to mononuclear fragments [55, 56]. The derivation of macroscopic magnetic properties is given in [57].

The current version of the POLY_ANISO program is able to calculate the following quantities:

- Anisotropic exchange interaction within the Lines model described above. Dipole–dipole magnetic interaction between centres is calculated fully *ab initio* and is added to the exchange matrix.
- Parameters of pseudospin magnetic Hamiltonians (see the description in Section 6.3.1, points 1–4). It is important to note that the multiplicity of the pseudospin can become quite large in the case of polynuclear compounds with weakly interacting magnetic sites.
- Static magnetic properties (see Section 6.3.1, points 1–4): The calculation of magnetic properties takes into account the contribution of all exchange states and also excited states on individual magnetic centres (the ligand field and charge transfer states of the complex or mononuclear fragment included in the RASSI calculation) via their thermal population and Zeeman admixture. The intermolecular exchange interaction between magnetic molecules in a crystal can be taken into account during the simulation of magnetic properties by a phenomenological parameter zJ' specified in the input.

6.4.4 Noncollinear Magnetic Structure of Ln_n Complexes

A prominent feature of polynuclear lanthanide complexes, which distinguishes them from TM complexes, is their noncollinear magnetic structure. TM complexes are usually found in the strong exchange limit [86], when the exchange splitting in the complex is much larger than the zero-field splitting on the metal sites. In such systems, the ionic and exchange anisotropy leads to zero-field splitting of exchange multiplets, characterized by a total spin S into individual levels or into exchange doublets $|S, \pm M\rangle$ (or their combinations) when the axial anisotropy of the entire complex is predominant, as in Mn_{12}acac and Fe_8 complexes [87]. In the state of saturated magnetization $+M$ or $-M$ of a given doublet, the local magnetizations on the metal sites (and radicals, if any) are parallel or antiparallel to its total magnetization, because the corresponding wave functions $|S, +M\rangle$ or $|S, -M\rangle$, are eigenstates of isotropic (Heisenberg) exchange interaction. Contrary to TM compounds, lanthanide complexes are found in the weak exchange limit because the CF splitting of the ground atomic multiplet of Ln ions ($> 500\text{cm}^{-1}$) exceeds considerably the exchange interaction between them (few per centimetres). As a result, in the case of lanthanides, which are in addition strongly axial ($g_Z \gg g_X, g_Y$) in low-symmetric environment, the local magnetizations in magnetically saturated states will point along the main magnetic axes (Z) of corresponding Ln ions, which are generally not parallel to each other.

As an example of such a noncollinear magnetic structure revealed by *ab initio* calculations, Figure 6.4 shows the calculated local anisotropy axes on three Dy sites of the Dy_3 triangle and the relative arrangement of the local magnetic moments in the ground state [60]. The three magnetic moments form an almost toroidal arrangement (Figure 6.4) and sum up into a total magnetic moment $<0.5\mu_B$ (calculated local magnetic moments on Dy sites are $\approx 10\mu_B$), in full

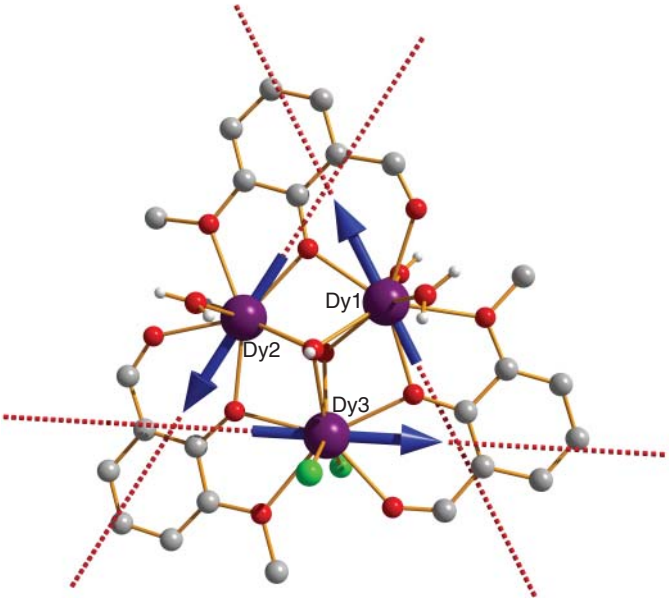

Figure 6.4 Structure of the Dy_3 triangular unit [60, 67]. Colour scheme: Dy^{III}, purple; Cl, green; O, red; C, grey; H, white. Dashed lines show the calculated anisotropy axes on the dysprosium sites and the arrows show the ordering of local magnetizations in the ground state of the complex.

accord with the experimental slope of $M(H)$ and χT at low temperature [59]. It is worth noting that besides a good description of magnetism, the applied *ab initio* methodology proved to be surprisingly accurate in the prediction of anisotropic properties of individual Ln ions. Thus, the Dy_3 triangle is the first molecular system where an almost perfect toroidal magnetic moment was detected. Indeed, the experimentally derived directions of local anisotropy axes [61] show deviations from the calculated ones by only a few degrees [67].

Another important insight offered by the *ab initio* calculations is the structure and the anisotropy of exchange multiplets of Dy_3 complex, arising from anisotropic exchange and dipolar interaction between Dy centres (Section 6.4.1). Figure 6.5 shows the spectrum of lowest exchange multiplets arising from the interaction between the ground KDs at Dy sites [67]. The three excited exchange multiplets correspond to reversal of one or two local magnetic moments with respect to the ground magnetic configuration (Figure 6.5c). As a result, the complex acquires in these states a magnetic moment of about 20 μ_B, which mostly lies in the Dy_3 plane as the Zeeman splitting shows (Figure 6.5a). The almost perfect cancellation of the sum of three magnetic moments in the ground state of dysprosium triangle is due to its nearly trigonal symmetry and to the fact that the local magnetic axes lie mostly in the Dy_3 plane (Figure 6.4). Deviation

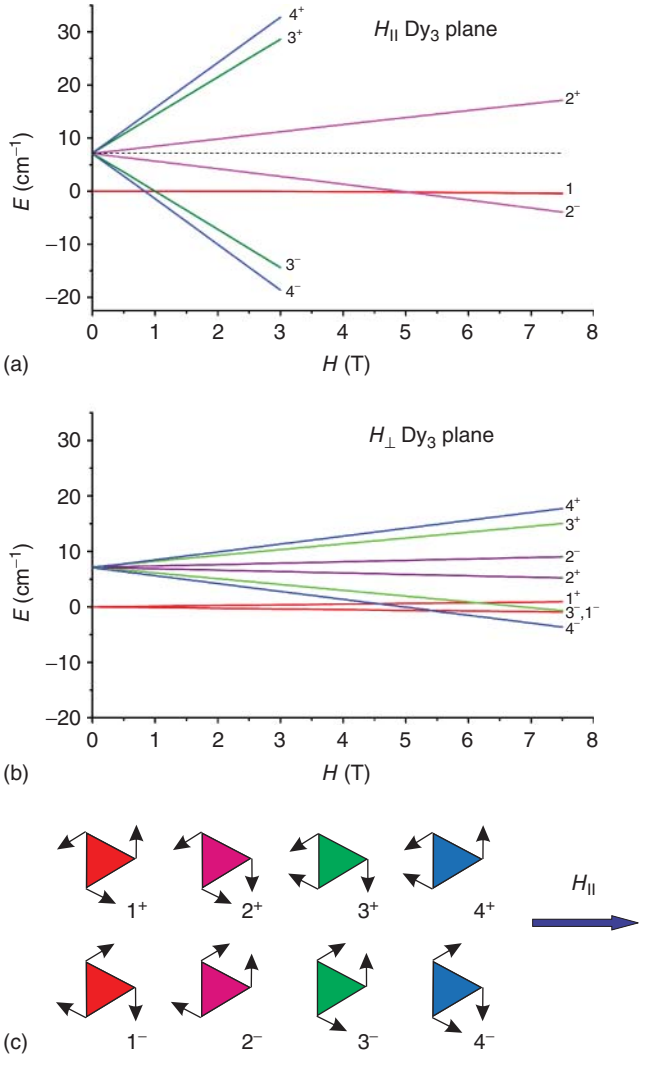

Figure 6.5 Evolution of the lowest magnetic states of Dy_3 complex with applied magnetic field, simulated for $J = -0.6$ cm^{-1}: (a) H is applied in the Dy_3 plane. Reproduced from Ref. [67] with permission from the Centre National de la Recherche Scientifique (CNRS) and The Royal Society of Chemistry; (b) H is perpendicular to the Dy_3 plane; (c) schematic noncollinear magnetic structure of the ground (1) and three excited (2–4) Kramers doublets and the direction of the in-plane applied field in (a). The two signs in the superscripts denote the two time reversal components of the Kramers doublets.

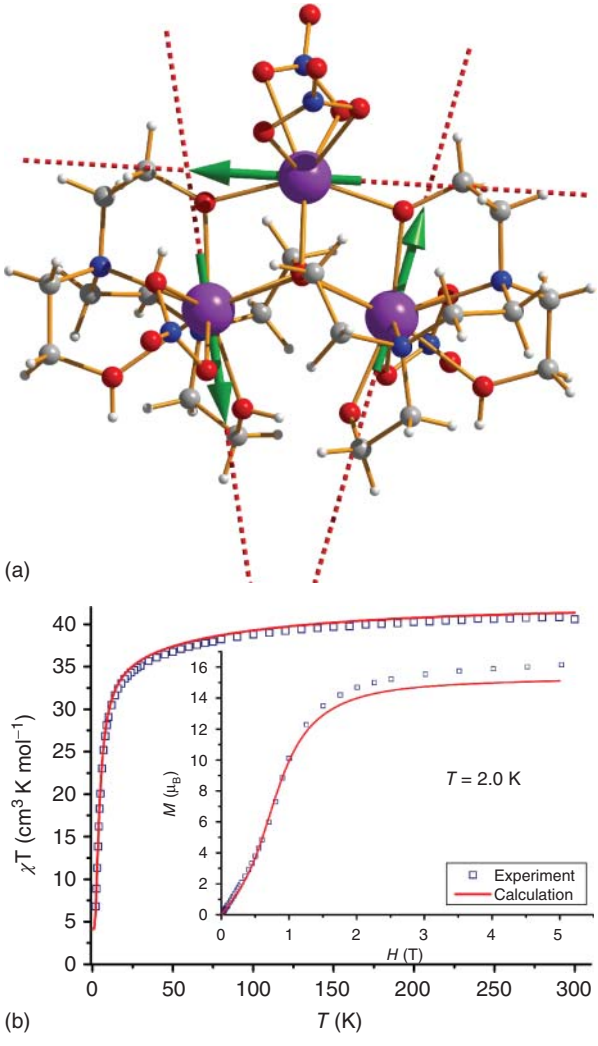

Figure 6.6 (a) Calculated local anisotropy axes on Dy(III) sites (dashed lines) and the local magnetic moments in the ground state (arrows). (b) Temperature dependence of the χT product for Dy_3-isoscelles complex. The red line is the *ab initio* calculated curve. Inset: molar magnetization at 2.0 K. (Reproduced from Ref. [72] with permission from The Royal Society of Chemistry.)

from the geometry of an equilateral triangle will destroy this cancellation resulting in a magnetic ground state of the complex. As an example, Figure 6.6 shows a complex where one oxygen bridge connecting two of three Dy centres is removed [72]. The calculated main magnetic axes in the ground KD of Dy(III) ions still lie

in the Dy_3 plane; however, the local magnetic moments in the ground exchange multiplet do not compensate each other anymore, resulting in a non-negligible total magnetic moment (Figure 6.6a). The latter manifests itself in a high slope of magnetization $M(H)$ and χT curves at low temperatures (Figure 6.6b). We also note that the *ab initio* methodology gives quite an accurate description of excited exchange multiplets, which is testified by close reproduction of experimental magnetization steps [72]. This approach was found successful also for the rationalization of anisotropic magnetic properties and the elucidation of non-collinear magnetic structure in a number of Ln_n complexes of higher nuclearity such as Dy_4 parallelogram [88] and Dy_6 wheel [71].

6.4.5 Mixed Lanthanide-Transition Metal Compounds

One of the intensively explored directions in the lanthanide research is the design of mixed lanthanide-TM compounds. The main motivation behind this research is the much stronger exchange interaction (by about one order of magnitude) in Ln–TM pairs compared to Ln–Ln pairs, which in combination with strong anisotropy on Ln sites, makes the mixed compounds more promising candidates for the design of efficient SMMs. The magnetic structure in the ground exchange multiplets of mixed compounds is richer than in pure lanthanide complexes and depends on the nature of TM ions and on the relative orientations of the main magnetic axes on Ln ions. Since the latter are strongly axial as a rule, the exchange interaction between them and isotropic TM ions (or radicals) is of collinear Ising type. Then, given that the Ln ions contained in the complex have all parallel main magnetic axes, the arrangements of all magnetic moments in the ground exchange doublet of mixed complex will be parallel, that is, fully collinear, with all local magnetic moments pointing along these axes. As an example, Figure 6.7a shows a $Cr_2^{III}Dy_2^{III}$ tetranuclear complex, where *ab initio* calculations have revealed such a magnetic structure [75]. If the local magnetic axes on Ln sites are not parallel to each other, then the isotropic spin of a TM, which interacts with two (or more) of them will align along an intermediate direction, to provide the maximal gain of exchange energy in the ground state. For example, in $Cr_4^{III}Dy_4^{III}$ square (wheel) complex (Figure 6.7b) the isotropic spin on each Cr ion lies in the plane bisecting the angle between the directions of the main magnetic axes of two neighbouring Dy sites [89]. Finally, when the TM ions are not isotropic, their magnetic moments in the ground exchange multiplet of the complex will not align completely to the magnetic axes of the lanthanide ions with which they interact, but will occupy an intermediate direction between the latter and their own anisotropy axes. As an example, Figure 6.7c shows the arrangement of local magnetic moments in the ground state of $Co_2^{II}Dy_2^{III}$ complex [70], from which we can see that the magnetic moments on Co ions are not parallel to the magnetic moments on Dy ions, albeit the latter have parallel magnetic axes.

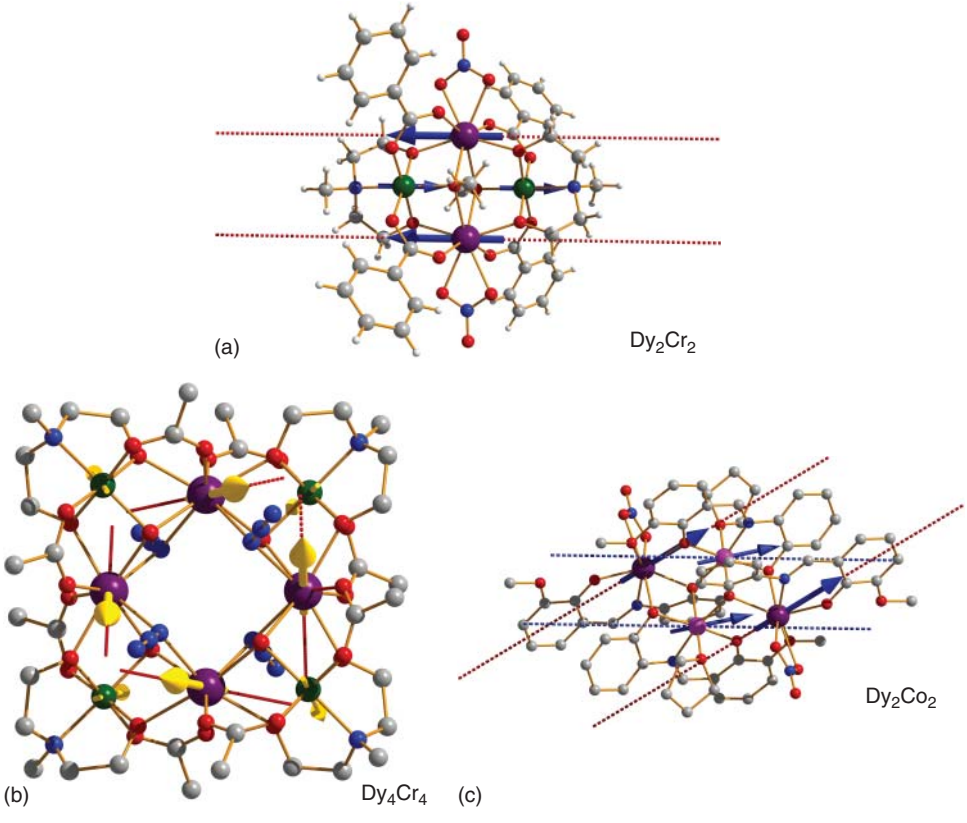

Figure 6.7 (a) Molecular structure of the $Dy^{III}_2Cr^{III}_2$ complex [75]. (b) Molecular structure of the $Dy^{III}_4Cr^{III}_4$ complex [89]. Copyright © 2010 WILEY VCH Verlag GmbH & Co. KGaA, Weinheim. (c) Molecular structure of the $Dy^{III}_2Co^{II}_2$ complex [70]. In (a), magnetic moments on Cr ions are exactly antiparallel to the moments on Dy^{III} ions due to inversion symmetry of the entire complex (i.e. main magnetic axes on Dy are parallel), strong Dy–Cr antiferromagnetic coupling and lack of intraionic anisotropy on Cr^{III} ions. In (b), the magnetic moments on Cr^{III} ions are oriented in between the magnetic moments of neighbouring Dy^{III} ions. In (c), there is a competition between exchange interaction, which tends to align all magnetic moments along a certain axis, and local magnetic anisotropy, which orients the magnetic moments on metal sites along their intrinsic anisotropy axes.

Another distinct property of mixed complexes which we mention here is the possibility to observe two activation regimes of relaxation of magnetization. One of them corresponds to reversal of magnetization of individual ions, at higher temperatures, and the other is related to climbing over the barrier built from the exchange multiplets of the complex. The coexistence of these two relaxation regimes has been recently revealed in the $Co^{II}_2Dy^{III}_2$ complex in a combined study

including ac susceptibility and recovery magnetization measurements and the *ab initio* calculations [70]. On the other hand, two activation barriers are not seen concomitantly in pure Ln_n complexes due to a weaker exchange/dipolar interaction and, as a consequence, a much lower exchange barrier. Besides providing relatively strong exchange interaction, the largest being recently attained in some $Ln_2(N_2)^{3-}$ lanthanide-radical systems [90, 91], the mixed complexes can involve isotropic magnetic centres with large spin, which is an additional factor contributing to the design of efficient barriers for magnetization blocking [73].

6.4.6 Lanthanide-Containing Magnetic Chains

It is well known that the magnetic properties of long (infinite) chains of exchange-coupled magnetic centres are generally not described exactly, even at a model level of theory. Two practical tools for the treatment of chains of isotropically (slightly anisotropically) coupled spins are the classical treatment in the case of large spins ($S \gg 1/2$) [92] or via Monte Carlo simulations [93]. Contrary to isotropic spin chains, the chains containing lanthanide ions allow for a surprising simplification of their theoretical description and, as a consequence, to an exact treatment of their magnetic properties in some important cases. These are situations when the chain can be divided into units delimited by strongly axial pseudospins described by the ground multiplets of Ln ions. It is supposed that these pseudospins have Ising exchange interactions with left and right (multicentre) units, while the latter do not interact directly. In this case, the thermodynamical properties of the chains can be calculated exactly by the transfer matrix method [94]. In combination with *ab initio* treatment of anisotropic magnetic properties of individual metal centres described above, this approach allows for the full treatment of magnetism in many Ln-containing magnetic chains. The approach described has been applied for the *ab initio* investigation of $\{[(CuL)_2Dy][Mo(CN)_8]\}_\infty$, the first studied chain with the 3d–4f–5d motif [66]. Figure 6.8a shows that the chain can be conceived as Cu1–Mo–Cu2 magnetic units linked via Dy(III) ions. The *ab initio* calculations have shown that the ground KD at each Dy(III) site is strongly axial [66]. Then, applying the transfer matrix method the magnetic susceptibility and field-dependent magnetization have been simulated (Figure 6.8b,c). The relative arrangement of magnetic moments on Dy sites in the ground state of the chain is shown in Figure 6.8a.

Another series of lanthanide-containing chains which have been treated *ab initio* are the chiral $\{Dy_3Cu\}_\infty$ 1D polymers [69]. These polymers represent Dy_3 units, with structure similar to the dysprosium triangles discussed above (Figure 6.4), linked via Cu(II) ions (Figure 6.9a). The latter are connected to Dy_2 ion in the right unit and to Dy_1 in the left one. The *ab initio* calculations show that all Dy ions in the units are strongly axial, with relative orientations of main magnetic axes very close to the dysprosium triangle (Figure 6.4). As in

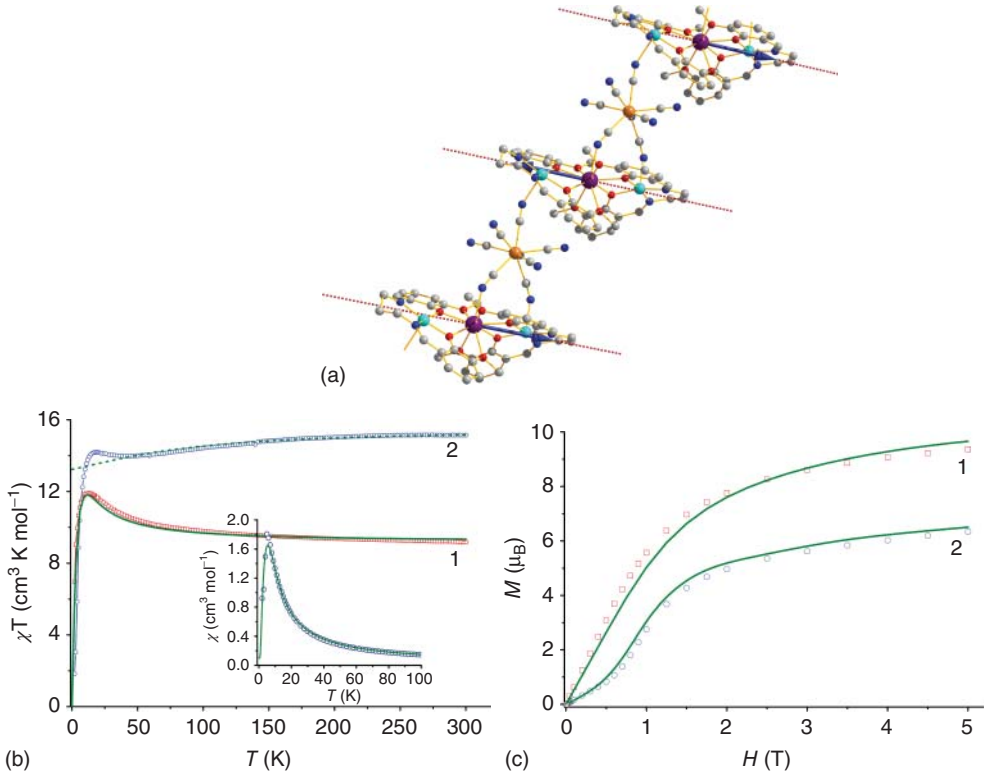

Figure 6.8 (a) Direction of local anisotropy axes (dashed lines) and the low-temperature alignment of magnetic moments (blue arrows) on dysprosium ions along the chain in crystal $\{[(CuL)_2Dy][Mo(CN)_8]\}_\infty$ [66]. (b) Temperature dependence of $\chi_M(T)$ for $\{[(CuL)_2Gd][Mo(CN)_8]\}_\infty$ (**1**) and $\{[(CuL)_2Dy][Mo(CN)_8]\}_\infty$ (**2**) (experimental in squares (**1**) and circles (**2**), and simulated in solid line), the dashed curve corresponds to *ab initio* calculation of $\chi_M(T)$ for non-interacting magnetic centres in **2**; the inset shows the experimental (circles) and simulated (line) susceptibility χ_M of (**2**) taking into account the exchange interaction between metal centres [66]. (c) Field dependence of the magnetization recorded for 2.0 K **1** (squares) and **2** (dots), the continuous curves are the *ab initio* based simulations for **1** and **2** when exchange interactions between magnetic ions is taken into account.

the latter case, the exchange/dipolar interaction between Dy centres stabilizes the toroidal arrangement of local magnetic moments in each Dy_3 unit. The calculated magnetic properties of the chain are shown in Figure 6.9b. The exchange spectrum and anisotropic magnetic properties of individual Dy_3 units is similar to those shown in Figure 6.5 for the dysprosium triangle. The spectrum of low-lying excitations in the chain corresponds to Ising exchange interaction between the ground state exchange KD of Dy_3 units, describing the two values

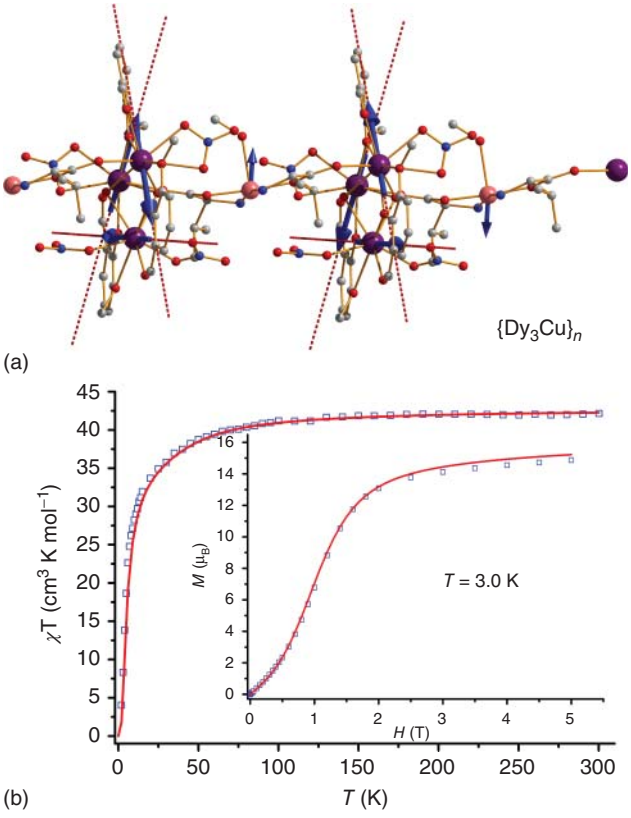

Figure 6.9 (a) Calculated anisotropy axes for the lowest Kramers doublets on Dy ions in the chiral $\{Dy_3Cu\}_\infty$ 1D polymers [69]. Blue arrows show the orientation of the local magnetic moments in the ground state on Dy and Cu ions. (b) A comparison between measured (empty squares) and calculated (red line) magnetic susceptibility for the $\{Dy_3Cu\}_\infty$ chain. Inset: a comparison of the measured and calculated molar magnetization at 3.0 K. (Reproduced from Ref. [69] with permission from The Royal Society of Chemistry.)

of the toroidal moment ($\tau = \pm 1/2$) and the projections of magnetic moment of Cu(II) ion ($s_z = 1/2$) along their direction in the ground state. (Figure 6.9a).

6.5 Conclusions

Theoretical description of molecular magnets has a history of several decades. The most investigated systems in the past were isotropic or weakly anisotropic magnetic molecules, for which the phenomenological modelling of their magnetic

properties was sufficient [86, 92]. The strongly anisotropic magnetic complexes, in particular, the lanthanide compounds, represent more complex magnetic properties requiring much more involved models for their rationalization. To be adequate, these models should involve tens of parameters, which can hardly be extracted from experiment in a reliable way. At this stage, the *ab initio* calculations based on explicitly correlated wave functions of the complex with non-perturbative (exact) treatment of spin–orbit coupling can become an indispensable research tool. We have shown here that the *ab initio* calculations based on CASSCF/RASSI approach implemented in MOLCAS package [13] provide the description of magnetic properties with experimental accuracy, while the pseudospin magnetic Hamiltonians describing these properties can be routinely derived from the results of these calculations. The *ab initio* approach is supplemented by phenomenological description of anisotropic exchange interactions within the Lines model, proved to be also highly successful for the description of many polynuclear compounds involving lanthanides. Given the constantly increasing computer power and predictive capabilities of modern quantum chemistry, the *ab initio* methods are expected to become a standard research tool for lanthanide-based magnetic materials.

References

1. Ishikawa, N., Sugita, M., Ishikawa, T., Koshihara, S. and Kaizu, Y. (2004) *J. Phys. Chem. B*, **108**, 11,265–11,271.
2. Woodruff, D.N., Winpenny, R.E.P. and Layfield, R.A. (2013) *Chem. Rev.*, **113**, 5110–5148.
3. Sessoli, R. and Powell, A.K. (2009) *Coord. Chem. Rev.*, **253**, 2328–2341.
4. Wybourne, B.G. (1965) *Spectroscopic Properties of Rare Earth Ions*, Interscience, New York.
5. Douglas, M. and Kroll, N.M. (1974) *Ann. Phys.*, **82**, 89–155.
6. Hess, B.A. (1986) *Phys. Rev. A*, **33**, 3742–3748.
7. Reiher, M. (2012) *WIREs Comput. Mol. Sci.*, **2**, 139–149.
8. Siegbahn, P.E.M., Heiberg, A., Roos, B.O. and Levy, B. (1980) *Phys. Scr.*, **21**, 323–327.
9. Roos, B.O., Taylor, P.R. and Siegbahn, P.E.M. (1980) *Chem. Phys.*, **48**, 157–173.
10. Siegbahn, P.E.M., Almlöf, J., Heiberg, A. and Roos, B.O. (1981) *J. Chem. Phys.*, **74**, 2384–2396.
11. Olsen, J., Roos, B.O., Jørgensen, P. and Jensen, H.J.A. (1988) *J. Chem. Phys.*, **89**, 2185.
12. Malmqvist, P.A.A., Rendall, A. and Roos, B.O. (1990) *J. Phys. Chem.*, **94**, 5477–5482.
13. Aquilante, F., Vico, L.D., Ferré, N., Ghigo, G., Malmqvist, P.A.A., Neogrády, P., Pedersen, T.B., Pitoňák, M., Reiher, M., Roos, B.O., Serrano-Andrés, L., Urban, M., Veryazov, V. and Lindh, R. (2010) *J. Comput. Chem.*, **31**, 224.
14. Frisch, M.J., Trucks, G.W., Schlegel, H.B., Scuseria, G.E., Robb, M.A. *et al.* (2009) *Gaussian 09 Revision A.1*, Gaussian Inc., Wallingford, CT.
15. Neese, F. (2010) *ORCA - An Ab Initio, Density Functional and Semiempirical Program Package, Version 2.9.0.*, Universitat Bonn, Bonn.
16. Werner, H.-J., Knowles, P.J., Manby, F.R., Schutz, M. *et al.* (2009) *MOLPRO, Version 2009.1, A Package of ab Initio Programs*, Universitat Stuttgart, Stuttgart, *http://www.molpro.net* (accessed 09 September 2014).

17. Andersson, K., Malmqvist, P.A.A. and Roos, B.O. (1992) *J. Chem. Phys.*, **96**, 1218.
18. Angeli, C., Cimiraglia, R., Evangelisti, S., Leininger, T. and Malrieu, J.P. (2001) *J. Chem. Phys.*, **114**, 10 252.
19. Roos, B.O., Andersson, K., Fulscher, M.P., Malmqvist, P.A.A., Serrano-Andres, L., Pierloot, K. and Merchan, M. (1996) *Adv. Chem. Phys.*, **93**, 219–331.
20. Schapiro, I., Sivalingam, K. and Neese, F. (2013) *J. Chem. Theory Comput.*, **9**, 3567-3580.
21. Helgaker, T., Olsen, J. and Jørgensen, P. (2000) *Molecular Electronic-Structure Theory*, John Wiley & Sons, Ltd.
22. Garcia, V.M., Castell, O., Caballol, R. and Malrieu, J.P. (1995) *Chem. Phys. Lett.*, **238**, 222-229.
23. Douglas, N. and Kroll, N.M. (1974) *Ann. Phys.*, **82**, 89.
24. Hess, B.A. (1986) *Phys. Rev. A*, **33**, 742.
25. Hess, B.A., Marian, C., Wahlgren, U. and Gropen, O. (1996) *Chem. Phys. Lett.*, **251**, 365.
26. Roos, B.O., Lindh, R., Malmqvist, P.A.A., Veryazov, V. and Widmark, P.O. (2004) *J. Phys. Chem. A*, **108**, 2851–2858.
27. Roos, B.O., Lindh, R., Malmqvist, P.A.A., Veryazov, V. and Widmark, P.O. (2005) *J. Phys. Chem. A*, **109**, 6575–6579.
28. Tsuchiya, T., Abe, M., Nakajima, T. and Hirao, K. (2001) *J. Chem. Phys.*, **115**, 4463.
29. Malmqvist, P.A.A., Roos, B.O. and Schimmelpfennig, B. (2002) *Chem. Phys. Lett.*, **357**, 230.
30. Ganyushin, D. and Neese, F. (2013) *J. Chem. Phys.*, **138**, 104 113.
31. Vallet, V., Maron, L., Teichteil, C. and Flament, J.P. (2000) *J. Chem. Phys.*, **113**, 1391–1402.
32. Verma, P. and Autschbach, J. (2013) *J. Chem. Theory Comput.*, **9**, 1052–1067.
33. Zalubas, W.C.M.R. and Hagan, L. (1978) *Atomic Energy Levels - The Rare-Earth Elements*, US Government Printing Office, Washington, DC.
34. Sandratskii, L.M. (1998) *Adv. Phys.*, **47**, 91–160.
35. Abragam, A. and Bleaney, B. (1970) *Electron Paramagnetic Resonance of Transition Ions*, Oxford University Press, Oxford.
36. Wigner, E.P. (1959) *Group Theory: And its Application to the Quantum Mechanics of Atomic Spectra*, Academic Press, London.
37. Ungur, L. and Chibotaru, L.F. (2011) *Phys. Chem. Chem. Phys.*, **13**, 20 086–20 090.
38. Ishikawa, N., Sugita, M., Ishikawa, T., Koshihara, S. and Kaizu, Y. (2003) *J. Am. Chem. Soc.*, **125**, 8694-8695.
39. AlDamen, M.A., Clemente-Juan, J.M., Coronado, E., Martí-Gastaldo, C. and Gaita-Ariño, A. (2008) *J. Am. Chem. Soc.*, **130**, 8874-8875.
40. Judd, B.R. (1963) *Operators Techiques in Atomic Spectroscopy*, McGraw-Hill.
41. Morrison, C.A. and Leavitt, R.P. (1982) *Handbook on the Physics and Chemistry of Rare Earths*, vol. 5, North-Holland, Amsterdam, pp. 461–692.
42. Jørgensen, C.K. (1963) *Adv. Chem. Phys.*, **5**, 33–146.
43. Gerloch, M. and Wooley, R.G. (1983) *Prog. Inorg. Chem.*, **31**, 371–446.
44. Figgis, B.N. and Hitchman, M.A. (1999) *Ligand Field Theory and its Applications*, Wiley-VCH Verlag GmbH.
45. Görller-Walrand, C. and Binnemans, K. (1996) *Handbook on the Physics and Chemistry of Rare Earths*, vol. 23, North-Holland, Amsterdam, pp. 121–283.
46. Erdos, P. and Razafimandimby, H.A. (1979) *J. Phys. (Paris)*, **40**, 171–172.
47. Newman, D.J. (1971) *Adv. Phys.*, **20**, 197–446.
48. Morrison, C.A. (1982) Lectures on Crystal Field Theory. Tech. Rep. HDL-SR-82-2, Harry Diamonds Laboratory.
49. Malta, O.L. (1982) *Chem. Phys. Lett.*, **87**, 27-29.
50. Malta, O.L. (1982) *Chem. Phys. Lett.*, **88**, 353–356.
51. Nekvasil, V. (1978) *Phys. Status Solidi B*, **87**, 317–323.
52. Nekvasil, V. (1979) *Czech. J. Phys.*, **88**, 785–796.
53. Petit, S., Pillet, G., Luneau, D., Chibotaru, L.F. and Ungur, L. (2007) *Dalton Trans.*, **40**, 4582–4588.

54. Boulon, M.E., Cucinotta, G., Luzon, J., DeglInnocenti, C., Perfetti, M., Bernot, K., Calvez, G., Caneschi, A. and Sessoli, R. (2013) *Angew. Chem. Int. Ed.*, **52**, 350–354.
55. Chibotaru, L.F. and Ungur, L. (2012) *J. Chem. Phys.*, **137**, 064 112.
56. Chibotaru, L.F. (2013) *Adv. Chem. Phys.*, **153**, 397–519.
57. Ungur, L. (2010) Ab initio methodology for the investigation of magnetism in strongly anisotropic complexes. PhD thesis, KU Leuven.
58. Feltham, H.L.C., Lan, Y., Klöwer, F., Ungur, L., Chibotaru, L.F., Powell, A.K. and Brooker, S. (2011) *Chem. Eur. J.*, **17**, 4362–4365.
59. Tang, J.K., Hewitt, I., Madhu, N.T., Chastanet, G., Wernsdorfer, W., Anson, C.E., Benelli, C., Sessoli, R. and Powell, A.K. (2006) *Angew. Chem. Int. Ed.*, **45**, 1729–1733.
60. Chibotaru, L.F., Ungur, L. and Soncini, A. (2008) *Angew. Chem. Int. Ed.*, **47**, 4126–4129.
61. Luzon, J., Bernot, K., Hewitt, I.J., Anson, C.E., Powell, A.K. and Sessoli, R. (2008) *Phys. Rev. Lett.*, **100**, 247 205.
62. Boulon, M.E., Cucinotta, G., Liu, S.S., Jiang, S.D., Ungur, L., Chibotaru, L.F., Gao, S. and Sessoli, R. (2013) *Chem. Eur. J.*, **19**, 13 726–13 731.
63. Bernot, K., Luzon, J., Bogani, L., Etienne, M., Sangregorio, C., Shanmugam, M., Caneschi, A., Sessoli, R. and Gatteschi, D. (2009) *J. Am. Chem. Soc.*, **131**, 5573–5579.
64. da Cunha, T.T., Jung, J., Boulon, M.E., Campo, G., Pointillart, F., Pereira, C.L.M., Guennic, B.L., Cador, O., Bernot, K., Pineider, F., Golhen, S. and Ouahab, L. (2013) *J. Am. Chem. Soc.*, **135**, 16 332–16 335.
65. Blagg, R.J., Ungur, L., Tuna, F., Speak, J., Comar, P., Collison, D., Wernsdorfer, W., McInnes, E.J.L., Chibotaru, L.F. and Winpenny, R.E.P. (2013) *Nat. Chem.*, **5**, 673-678.
66. Visinescu, D., Madalan, A.M., Andruh, M., Duhayon, C., Sutter, J.P., Ungur, L., den Heuvel, W.V., and Chibotaru, L.F. (2009) *Chem. Eur. J.*, **15**, 11 808–11 814.
67. Ungur, L., den Heuvel, W.V. and Chibotaru, L.F. (2009) *New J. Chem.*, **33**, 1224-1230.
68. Guo, Y.N., Xu, G.F., Wernsdorfer, W., Ungur, L., Guo, Y., Tang, J., Zhang, H.J., Chibotaru, L.F. and Powell, A.K. (2011) *J. Am. Chem. Soc.*, **133**, 11 948–11 951.
69. Novitchi, G., Pilet, G., Ungur, L., Moshchalkov, V.V., Wernsdorfer, W., Chibotaru, L., Luneau, D. and Powell, A.K. (2012) *Chem. Sci.*, **3**, 1169–1176.
70. Mondal, K.C., Sundt, A., Lan, Y., Kostakis, G.E., Waldmann, O., Ungur, L., Chibotaru, L.F., Anson, C.E. and Powell, A.K. (2012) *Angew. Chem. Int. Ed.*, **51**, 7550-7554.
71. Ungur, L., Langley, S.K., Hooper, T.N., Moubaraki, B., Brechin, E.K., Murray, K.S. and Chibotaru, L.F. (2012) *J. Am. Chem. Soc.*, **134**, 18 554–18 557.
72. Wang, Y.X., Shi, W., Li, H., Song, Y., Fang, L., Lan, Y.H., Powell, A.K., Wernsdorfer, W., Ungur, L., Chibotaru, L.F., Shen, M.R. and Cheng, P. (2012) *Chem. Sci.*, **3**, 3366–3370.
73. Ungur, L., Thewissen, M., Costes, J.P., Wernsdorfer, W. and Chibotaru, L.F. (2013) *Inorg. Chem.*, **52**, 6328-6337.
74. Vieru, V., Ungur, L. and Chibotaru, L.F. (2013) *J. Phys. Chem. Lett.*, **4**, 3565-3569.
75. Langley, S.K., Wielechowski, D.P., Vieru, V., Chilton, N.F., Moubaraki, B., Abrahams, B.F., Chibotaru, L.F. and Murray, K.S. (2013) *Angew. Chem. Int. Ed.*, **52**, 12 014–12 019.
76. Guo, F.S., Leng, J.D., Lin, Z., Tong, M.L., Song, G., Ungur, L. and Chibotaru, L.F. (2011) *Chem. Eur. J.*, **17**, 2458–2466.
77. Griffith, J.S. (1963) *Phys. Rev.*, **132**, 316.
78. Reu, O.S., Palii, A.V., Ostrovsky, S.M., Tregenna-Piggott, P.L.W. and Klokishner, S.I. (2012) *Inorg. Chem.*, **51**, 10 955-10 965.
79. Chilton, N.F., Collison, D., McInnes, E.J.L., Winpenny, R.E.P. and Soncini, A. (2013) *Nat. Commun.*, **4**, 2551.
80. Ungur, L. and Chibotaru, L.F. (2014) *Chem. Sci.*, submitted.
81. Ungur, L. and Chibotaru, L.F. (2006-2013) *SINGLE_ANISO Program*, KU Leuven, Belgium, *http://www.molcas.org* (accessed 09 September 2014).

82. Rajamaran, G., Totti, F., Bencini, A., Caneschi, A., Sessoli, R. and Gatteschi, D. (2009) *J. Comput. Chem.*, **17**, 3153–3161.

83. Anderson, P.W. (1959) *Phys. Rev.*, **115**, 2–13.

84. Lines, M. (1971) *J. Chem. Phys.*, **55**, 2977.

85. Cucinotta, G., Perfetti, M., Luzon, J., Etienne, M., Car, P.E., Caneschi, A., Calvez, G., Bernot, K. and Sessoli, R. (2012) *Angew. Chem. Int. Ed.*, **51**, 1606–1610.

86. Bencini, A. and Gatteschi, D. (1990) *Electron Paramagnetic Resonance of Exchange Coupled Systems*, Springer.

87. Gatteschi, D., Sessoli, R. and Villain, J. (2006) *Molecular Nanomagnets*, Oxford University Press.

88. Guo, P.H., Liu, J.L., Zhang, Z.M., Ungur, L., Chibotaru, L.F., Leng, J.D., Guo, F.S. and Tong, M.L. (2012) *Inorg. Chem.*, **51**, 1233–1235.

89. Rinck, J., Novitchi, G., van den Heuvel, W., Ungur, L., Lan, Y., Wernsdorfer, W., Anson, C.E., Chibotaru, L.F. and Powell, A.K. (2010) *Angew. Chem. Int. Ed.*, **49**, 7583–7587.

90. Rinehart, J.D., Fang, M., Evans, W.J. and Long, J.R. (2011) *Nat. Chem.*, **3**, 538–542.

91. Rinehart, J.D., Fang, M., Evans, W.J. and Long, J.R. (2011) *J. Am. Chem. Soc.*, **133**, 14 236-14 239.

92. Kahn, O. (1993) *Molecular Magnetism*, VCH Publishers, New York.

93. Cano, J. and Journaux, Y. (2005) *Magnetism: Molecules to Materials*, vol. 6, Wiley-VCH Verlag GmbH, pp. 189–222.

94. Van den Heuvel, W. and Chibotaru, L.F. (2010) *Phys. Rev. B*, **82**, 174,436.